Gamma-Ray Lidar (GRAYDAR) in-Depth Sensing of Optically Opaque Media

L. L. Gurdev[1], **T. N. Dreischuh**[1], **D. V. Stoyanov**[1],
Ch. N. Protochristov[2]

[1] Institute of Electronics, Bulgarian Academy of Sciences,
  Tsarigradsko Chaussee 72, BG-1784, Sofia, Bulgaria

[2] Institute for Nuclear Research and Nuclear Energy, Bulgarian Academy of
  Sciences, Tsarigradsko Chaussee 72, BG-1784, Sofia, Bulgaria

Abstract. Recently we proposed and investigated the feasibility of a novel approach for gamma-ray single-sided in-depth sensing and tomography of dense optically opaque media. The approach is based on graydar (Gamma RAY Detection And Ranging) principle, that is, time-to-range resolved detection of the backscattering-due radiative returns from the probed object irradiated by pulsed gamma-photon pencil beams. It was shown analytically and by simulations that under Poisson noise conditions such an approach would enable one, at reasonable sensing-photon fluxes and measurement time intervals, to accurately determine the location, the material content, and the mass density of homogeneous ingredients within homogeneous surroundings as well as the mass (or electron) density distribution within one-material objects. At the same time, being quite general, the idea of graydar sensing should have considerably wider applied potential. In the present work we make a step to extending our knowledge about the applicability of the graydar approach. Concretely, we have investigated by simulations based on some theoretical reasons the possibility of detecting and characterizing homogeneous one-material ingredients in one-material surroundings with non-uniform spatial density distribution. As a result it is shown that one may find, locate and recognize, without noticeable shadowing effect, homogeneous one-material objects with relatively low contrast (say, the components of plastic landmines) hidden in one-material medium (say, soil) with strongly spatially varying density.

1 Introduction

The high-energy (gamma or X-rays) photons interact with the electron and nuclear structures of atoms through various elementary absorption and scattering processes [1–3]. The character and the intensity of these processes is conditioned by the photon energy and, specifically, by the kind and the density of atoms of the related material. This fact underlies different single-sided

and high-resolution gamma or X-ray techniques (methods) [4–12] for non-destructive evaluation of material substances that are not transparent for optical or microwave radiation. These methods are intended for determination of the electron-density distribution within the investigated objects and are usually based on the dependence of the energy of the Compton single-scattered photons on the angle of scattering. A common difficulty here is the lack of any clear approach for taking into account the extinction within the object. Besides, some of the methods [7–12] require too complicated image-reconstruction algorithms like those in computer-aided tomography [13–15]. Other ones [4–6] require relatively long data-collection time.

The graydar (Gamma RAY Detection And Ranging) approach [16–18] is free of the above-mentioned difficulties. It would allow one in principle to determine simultaneously, in a relatively simple unambiguous one-sided way and with controllable accuracy and resolution, the distributions of the extinction (linear attenuation) and (Compton or annihilation) backscattering coefficients within an object of interest. In turn, the knowledge of both the distributions should allow one to determine the distribution, inside the object, of different substances and their mass density.

The theoretical basis of the graydar approach has been developed in Ref. [16], where we have formulated the graydar principle and the graydar equation. We have also proposed and discussed there some ways of ensuring δ-pulse sensing under single-scattering conditions, and thus of ensuring the validity of the (δ-pulse single-backscattering) graydar equation. The capabilities of the graydar sensing have been demonstrated in two typical cases. In the first case the graydar line of sight (LOS, sensing beam axis) penetrates homogeneous regions (with constant extinction and backscattering coefficients) of different substances. In the second case the probed object consists of only one material having nonuniform spatial density distribution. On the basis of the graydar equation we have obtained, for both the cases, analytical rules and expressions for determination of the extinction and backscattering coefficient profiles along the LOS and the corresponding statistical and systematic errors due to Poisson noise. The simulations performed confirmed the analytical results and showed that, from a statistical point of view, one may realize gamma-ray single-sided, in-depth sensing and tomography of optically-opaque, dense media, achieving depths of sensing of the order of centimeters and decimeters at $\sim 10^5 - 10^7$ photons/s sensing fluxes of gamma-photons (of energy 511 KeV) and $\sim 10^4 - 10^2$ s measurement time.

The procedure of laterally scanning the LOS and obtaining two-dimensional (2D) images (sections) of the probed objects is simulated in Refs. [17] and [18]. In the former work it is shown that, at a number of 10^9 sensing photons deposited along one LOS, one may establish (with 2-3 mm longitudinal and transversal resolution) the presence, the disposition, the shape, and the kind of different homogeneous ingredients, cavities and flaws within a homogeneous surround-

ing material (aluminum); the presence of more than one flaw along one LOS is shown to not lead to noticeable shadowing effect. In the latter work it is shown that the approach is capable of finding, identifying, and imaging down to 5% density-contrast, homogeneous ingredients (plastic TNT landmines) in homogeneous soil, at depths to 20 cm, with spatial resolution of 1 to 10 mm, for measurement time of 10 to 1000 s, and positron-emission activity of the positron source of 50 - 300 mCi.

The main purpose of the present work is, after a brief review on the leading ideas and some recent results concerning the graydar approach, to investigate analytically and by simulations the peculiarities of a more general case of graydar sensing compared to those mentioned above. This is the case when one should detect and evaluate homogeneous ingredients (*e.g.*, explosives) hidden in one-material surroundings (soil) with non-uniform density distribution.

2 Theoretical Description of the Graydar Approach

2.1 Graydar Principle

Like the lidar (LIght Detection And Ranging) principle, the graydar principle consists in general in time-to-range resolved detection of the backscattering-due radiative (gamma-ray) return from a probed object irradiated by narrow-beam, pulsed gamma radiation (Figure 1). Considering commonly an inelastic scattering process, we may denote the incident-photon energy by E_f, and the return-photon energy by E_b. During the detection procedure the radiative return is transformed into an electrical signal (return signal) $F(t)$ measured as a function of the time delay t after the instant of emission of the corresponding sensing pulse. Under single-scattering conditions there exists one-to-one correspondence $t \equiv 2z/c$ ($z \equiv ct/2$) between the time t and the LOS distance z to the sensing-pulse front that is the front of the scattering volume contributing to the signal at this time; c is the speed of light. Also, if Δt is the sampling interval in the time domain, $\Delta z = c\Delta t/2$ will be the sampling interval in the range (along the LOS) domain. Thus we will obtain, in practice, a time-to-range resolved graydar (return signal) profile $F = F(t = 2z/c, \Delta t = 2\Delta z/c) = F(z =$
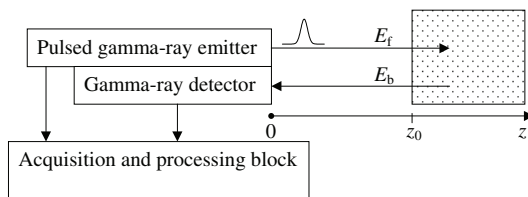

Figure 1. Illustration of the graydar principle.

$ct/2, \Delta z = c\Delta t/2$). The main theoretical instrument (for quantitative analysis) concerning graydar is the so-called graydar equation [16] that describes the relation between the graydar profile $F(t = 2z/c, \Delta t = 2\Delta z/c)$ and the parameters of the radiation-transceiving system, the energy E_f of the sensing gamma photons, and the LOS distribution of the physical characteristics (extinction and backscattering coefficients) of the medium under investigation. The most useful (leading to clearest results) form of the graydar equation is obtainable when the pulse length $l_p = c\tau_p$ (τ_p is the pulse duration) and Δz are smaller than the least variation scale of the material characteristics inside the probed object. In this case the timing uncertainty Δt_{u} due to inertness and noise in the transceiving electronics should be less than Δt [16]. As an idealization, we shall further assume that $\Delta t_{\mathrm{u}} << \Delta t$. Since it has not been possible so far to generate sufficiently short gamma-ray pulses (*e.g.*, with $\tau_p \sim 100$ ns) with a high (say 10^5) number of photons per pulse, we have proposed to use an approach [16, 19, 20] based on employing annihilation-photon pairs for realization of a gamma-ray δ-pulse-like sensing procedure. This approach is briefly described in the following subsection 2.2. The scattering mechanism of concern here will be the Compton effect. In this case there are two mutually complementary ways of selecting the single-backscattering photons alone. The first way consists in ensuring as narrow as possible field of view of the radiation-receiving system. At the same time, the field of view should cover the sensing photon beam in order to avoid the loss of signal (single-backscattered) photons. Thus, the transversal beam size determines the possible minimum transversal-resolution cell that is important, *e.g.*, when laterally scanning the LOS to obtain 2D or 3D (three-dimensional) images of the internal structure of the probed object [The achievable minimum range-resolution cell (along the LOS) is equal to Δz.] The other way for separation of the signal photons is based on the dependence of the energy of the Compton-scattered photons on the scattering angle. So, according to the Compton formula (*e.g.*, [1]), for $E_{\mathrm{f}} = 511$ KeV the signal (once only backscattered) photons will have (Compton) energy $E_{\mathrm{bc}} \cong 170$ KeV. Consequently, the signal photons would mostly be those of the detected ones whose energy is close upon 170 KeV. The energy selection of the signal photons would be effective when sensing light to medium-weight materials. For heavy materials there will be a relatively large [21, 22] Doppler broadening of the signal-photon energy spectrum around the Compton energy E_{bc}. Then the energy-selection approach seems to not be of use. In any case, this question requires a separate profound investigation.

2.2 Graydar Equation

Consider a monostatic sensing system emitting a narrow beam of gamma photons of energy E_{f} (incident on the probed object) and detecting the Compton backward-scattered photons of energy E_{bc}. The mean incident photon rate and the total measurement time (the duration of the sensing procedure) will be de-
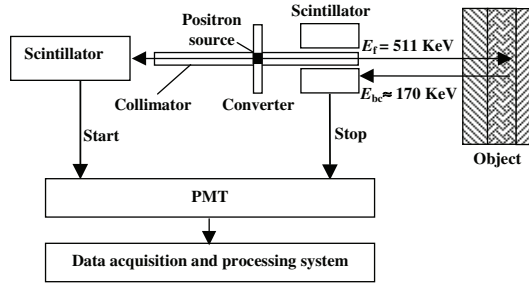
Figure 2. Principle block-scheme of experimental arrangement for gamma-ray lidar-type in-depth sensing of optically opaque media.

noted by q_0 and T, respectively. Further, one may consider each incident photon as a δ-like sensing pulse and specify the corresponding eventual registered signal photon by its energy $E_{\mathrm{b}} = E_{\mathrm{bc}}$ and arrival time t (with respect to the instant of emission of the sensing photon). To mark the instants of emission of the incident photons one may use [16, 19, 20] sensing photon beams resulting from electron-positron annihilation within a converter irradiated by positrons from a radioactive source (Figure 2). As a result of annihilation, two gamma photons of energy $E_{\mathrm{f}} = 511\,\mathrm{KeV}$ are simultaneously emitted in opposite directions. A portion of the continuously emitted photons is formed as a sensing beam and directed through a collimator to the probed object. The backpropagating photon of each "sensing" pair through the collimator reaches a scintillator and generates a start light pulse. The corresponding signal (once only backscattered) Compton photon of energy $E_{\mathrm{b}} \cong E_{\mathrm{bc}} = E_{\mathrm{f}}/3$ reaches another scintillator and produces a stop light pulse. Both the light pulses produce in turn, through a photomultiplier, a couple of two time-shifted electronic (start and stop) pulses. These output pulses are further amplified and processed to determine simultaneously both the energy and the arrival time of each detected photon. If z_{m} is the maximum LOS range within the investigated object, the maximum arrival time from it will be $\tau_{\mathrm{am}} = 2z_{\mathrm{m}}/c$. The mean time interval between two successive incident photons is $\tau_{\mathrm{m}} = q_0^{-1}$. When the time-coincidence condition $t < \tau_{\mathrm{am}} \ll \tau_{\mathrm{m}}$ is satisfied one can most probably expect that the acts of sensing-photon emission and return-photon detection are unambiguously connected. During the measurement period T, into the probed object, along one LOS, will be deposited $q_0 T$ sensing photons. At the same time one will obtain a realization $\widehat{N}_{\mathrm{T}}(E_{\mathrm{bc}}, t = 2z/c, \Delta t = 2\Delta z/c)$ of the energy-selected time-to-range resolved graydar profile $N_{\mathrm{T}}(E_{\mathrm{bc}}, t = 2z/c, \Delta t = 2\Delta z/c)$ describing the mean number of accumulated signal (at energy E_{bc}) gamma-photon counts per one resolution cell $\Delta t = 2\Delta z/c$ with arrival times between t and $t + \Delta t$ corresponding to acts of backscattering between the points z and $z + \Delta z$ along the

LOS. The graydar profile is described by the following **graydar** equation [16]:

$$N_{\mathrm{T}}(E_{\mathrm{bc}}, t, \Delta t) \equiv N_{\mathrm{T}}(E_{\mathrm{bc}}, z, \Delta z)$$
$$= dq_0 \Delta z T z^{-2} \, \eta(z)\beta(z) \exp\{-\int_{z_0}^{z} \mathrm{d}z' \, \alpha(z')\} = dq_0 \Delta z T z^{-2} \, \eta(z)S(z), \quad (1)$$

where $S(z) = \beta(z) \exp\{-\int_{z_0}^{z} \mathrm{d}z' \, \alpha(z')\}$ is the so-called (in the lidar practice) S- function, $d = \pi(r_{\mathrm{d}}^2 - r_{\mathrm{c}}^2)$, r_{d} and r_{c} ($<< r_{\mathrm{d}}$) are respectively the radii of the (circular) scintillating detector's layer and collimator's aperture, z_0 is the longitudinal coordinate of the "entrance" into the investigated object (see Figure 1), $\eta(z)$ is the receiving efficiency of the experimental setup that is usually equal to unity [16], $\beta(z)$ [m^{-1}/sr] is the LOS profile of the volume backscattering coefficient, and $\alpha(z) = \alpha_{\mathrm{f}}(z) + \alpha_{\mathrm{b}}(z)$ is the profile of the two-way extinction (linear attenuation) index, $\alpha_{\mathrm{f}}(z)$ [m^{-1}] and $\alpha_{\mathrm{b}}(z)$ [m^{-1}] are the extinction (linear attenuation) coefficients for the incident and signal photons, respectively. Equation (1) is the maximum-resolved (δ-pulse) single-backscattering graydar equation. It is valid when one use δ-like incident pulses, narrow-enough (matching the incident photon beam) field of view of the signal-photon receiver, sufficiently fast and precise photon-registration electronics ($\Delta t_{\mathrm{u}} << \Delta t$), and photon-energy analyzers of nearly ideal energy resolution. In the further analysis we shall assume that these validity conditions are satisfied and only the photon-counting Poisson noise disturbs the measurement process.

The graydar equation (1) contains two unknown functions, the profiles $\beta(z)$ and $\alpha(z)$, that comprise information about the material properties along the LOS. Consequently, to solve this equation with respect to $\alpha(z)$ and $\beta(z)$ one should use some additional prior to the experiment or posterior information about the investigated object or the measurement conditions. Based on this conception, as mentioned above, in Ref. [16] we have solved Eq.(1) in two cases. In the first case the LOS penetrates alternating homogeneous one-material regions. Then, within each region, the logarithm of the graydar profile is a decreasing linear function of z with a slope equal to the linear attenuation coefficient. In this case, the linear tendency revealed by the experimental data is the posterior information indicating each homogeneous region. In the second case, as a prior information, the probed object is assumed as consisting of one only material with possibly non-uniform mass density. Then the ratio of the extinction coefficient to the backscattering one is constant.

In the following analysis we shall continue and generalize the above-described preceding investigations and results. Namely, we shall investigate analytically and by simulations the potentialities of the (one- and two-dimensional) lidar-type gamma-ray sensing of one-material media with non-uniform density distribution containing homogeneous one-material ingredients.

3 Single-Sided Graydar Sensing and Tomography of One-Material Media with Spatially-Varying Density Containing Homogeneous Ingredients

In this case a sensing gamma-photon pencil beam would intersect one-material homogeneous regions $\Delta_i = [z_{i,1}, z_{i,2}]$ $(i = 1, 2, ...j)$ with constant backscattering and two-way extinction coefficients, β_i and α_i, respectively (see Figure 3). The space out of these regions (the intervals $[z_0, z_{1,1}]$, $[z_{1,2}, z_{2,1}]$, $[z_{2,2}, z_{3,1}]$,..., $[z_{j-1,2}, z_{j,1}]$, $[z_{j,2}, z_m]$) is assumed to be occupied by some one-material substance with non-uniform density distribution. At the same time, the graydar ratio b in this surrounding space is constant, that is, $b = \beta(z)/\alpha(z) = const$; $\beta(z)$ and $\alpha(z)$ are, respectively, the LOS profiles of the backscattering and the two-way extinction coefficient of the surrounding substance.

The length of a homogeneous one-material region Δ_i is obviously equal to $l_i = z_{i,2} - z_{i,1}$. Taking the logarithm of the graydar equation (1), for such a region we obtain [16, 18]

$$\ln S(z) = \ln \beta_i - \int_{z_0}^{z_{i,1}} \alpha(z') \mathrm{d}z' - (z - z_{i,1})\alpha_i \,. \tag{2}$$

Equation (2) shows that within each region Δ_i the logarithm $\ln S(z)$ decreases linearly with z, with a slope α_i. When the experimental data suggest a linear tendency in the behaviour of $\ln S(z)$ within some interval Δ_i, one can use two-parametric linear regression analysis (straight-line least-square approximation) of $\ln S(z)$ to determine α_i. In this case, the root-mean-square (rms) error in the determination of α_i is obtained as [16, 23]

$$\delta \alpha_i = l_i^{-1} \{ \sum_{p=0}^{q_i-1} N_p p^2/q_i^2 - (\sum_{p=0}^{q_i-1} N_p p/q_i)^2/(\sum_{p=0}^{q_i-1} N_p) \}^{-1/2} \,, \tag{3}$$

where $q_i = l_i/\Delta z$, and N_p is the value of N_{T} in the pth voxel within Δ_i. Eq. (3) is derived by using the fact that at large-enough values of N_{T} (say, $N_{\mathrm{T}} > 5$) the fluctuations of $\ln S$ are practically equal to the relative photon count fluctuations
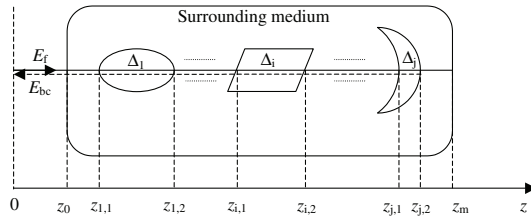

Figure 3. Illustration of sensing one-material medium with non-uniform density distribution containing homogeneous one-material ingredients.

$(\widehat{N_\mathrm{T}} - N_\mathrm{T})/N_\mathrm{T}$ whose variance is $\langle [(\widehat{N_\mathrm{T}} - N_\mathrm{T})/N_\mathrm{T}]^2 \rangle = N_\mathrm{T}^{-1}$; $\langle . \rangle$ denotes the ensemble average, and $N_\mathrm{T} = \langle \widehat{N_\mathrm{T}} \rangle$.

Let us further consider the solution of Eq.(1), with respect to $\alpha(z)$, for the surrounding area (out of the regions Δ_i), *e.g.* (most generally), in the interval $[z_{k,2}, z_{k+1,1}]$ between Δ_k and Δ_{k+1}. In this case ($b = const$) for $\alpha(z)$ we obtain

$$\alpha(z) = S_1(z)/\{\exp\left[-\int_{z_0}^{z_{k,2}} \alpha(z')\mathrm{d}z'\right] - \int_{z_{k,2}}^{z} S_1(z')\mathrm{d}z'\}. \qquad (4)$$

where $S_1(z) = S(z)/b$, and $\exp\left[-\int_{z_0}^{z_{k,2}} \alpha(z')\mathrm{d}z'\right] = \exp[-\int_{z_0}^{z_{1,1}} \alpha(z')\mathrm{d}z' - \sum_{i=1}^{k-1} \int_{z_{i,2}}^{z_{i+1,1}} \alpha(z')\mathrm{d}z' - \sum_{i=1}^{k} l_i \alpha_i]$. According to Eq.(4), an estimate $\widehat{\alpha}(z)$ of $\alpha(z)$ is obtainable in the form

$$\widehat{\alpha}(z) = \widehat{S}_1(z)/\{\exp\left[-\int_{z_0}^{z_{k,2}} \widehat{\alpha}(z')\mathrm{d}z'\right] - \int_{z_{k,2}}^{z} \widehat{S}_1(z')\mathrm{d}z'\}, \qquad (5)$$

where $\widehat{S}_1(z)$ is an experimental realization of $S_1(z)$, and $\widehat{\alpha}(z')$ denotes the corresponding estimates of $\alpha(z')$ first obtained for $z' < z_{k,2}$. Because of the complicated non-local, recurrent character of the expression of $\alpha(z)$ [see Eqs.(4) and (5)], the root-mean-square (rms) error $\delta\alpha = \langle [\widehat{\alpha}(z) - \alpha(z)]^2 \rangle^{1/2}$ cannot be derived in a compact and clear, physically viewable form. The behaviour of this error, depending on z, will be traced below in the results from simulations. In any case one may expect that, like in [16], it will be accumulated and will strongly increase with increasing z. So far as $\beta(z) = b\alpha(z)$, the corresponding estimate $\widehat{\beta}(z)$ based on the same experimental realization $\widehat{S}_1(z)$ will be $\widehat{\beta}(z) = b\widehat{\alpha}(z)$. The rms error $\delta\beta(z)$ in the determination of $\beta(z)$ will obviously be equal to $\delta\beta(z) = b\delta\alpha(z)$, and the relative errors $\delta\beta(z)/\beta(z)$ and $\delta\alpha(z)/\alpha(z)$ will obviously coincide, that is, $\delta\alpha(z)/\alpha(z) \equiv \delta\beta(z)/\beta(z)$. With the same accuracy, the recovered profile $\rho_r(z)$ of the mass-density distribution $\rho(z)$ of the surrounding matter is assessible as [16] $\rho_r(z) = \widehat{\alpha}(z)/(\mu_\mathrm{f} + \mu_\mathrm{b})$, where μ_f and μ_b are the mass attenuation coefficients for the incident and the signal photons, respectively.

Let us mention at last that, based on Eq.(1), the expression of the backscattering coefficient β_k for each homogeneous one-material region Δ_k is obtained in the form

$$\beta_k = S(z = z_{k,1}) \exp\left[-\int_{z_0}^{z_{1,1}} \alpha(z')\mathrm{d}z' - \sum_{i=1}^{k-1} \int_{z_{i,2}}^{z_{i+1,1}} \alpha(z')\mathrm{d}z' - \sum_{i=1}^{k} l_i \alpha_i\right]. \quad (6)$$

According to Eq.(6), the error $\delta\beta_k$ in the determination of β_k should depend on (accumulating) the error $\delta\alpha(z)$. Therefore it would be impossible to find any clear explicit expression of $\delta\beta_k$ [see above the comments about $\delta\alpha(z)$]. Thus,

the behaviour of $\delta\beta_k$ is expedient in principle to be studied by simulations. In the following analysis, based mainly on computer simulations, we shall mostly concentrate our attention on tomographic problems requiring the determination of the spatial distribution of the extinction coefficient α alone. Assuming sufficiently fine signal-photon discrimination and fast data acquisition and processing, we shall simulate only the Poisson-noise influence on the imaging process.

4 Simulations

To study and illustrate the possibilities of detecting, locating, and identifying homogeneous objects hidden in inhomogeneous one-material media, we shall consider a model of a plastic TNT landmine buried in a silty soil [24] with spatially varying mass density. Since the influence of the airy component of soil on the processes of scattering and absorption of gamma rays would be negligible, one may interpret the varying mass density as due to varying porosity. The photon count fluctuations are simulated on the basis of the assumption that they have Poisson statistics. Then the only parameter of importance is given by the graydar profile. This is the mean number of photon counts $N_{\mathrm{T}}(E_{\mathrm{bc}}, t = 2z/c, \Delta t = 2\Delta z/c)$ accumulated for the measurement period T and corresponding to acts of backscattering between z and $z + \Delta z$. At given models of $\alpha(z)$ and $\beta(z)$ (including α_i and β_i), the model of the mean graydar profile is calculated according to Eq.(1). Then its realizations are obtained by using a Poisson random-number generator. A schematic drawing illustrating the detection and characterization of the landmine is shown in Figure 4. The simulated experimental parameters are chosen to be: $z_0 = 10$ cm, $\Delta z = 1\,\mathrm{mm}$, $r_{\mathrm{d}} = 2.5$ cm, $r_{\mathrm{c}} = 0.1$ cm, $E_{\mathrm{f}} = 511\,\mathrm{KeV}$, $E_{\mathrm{bc}} = 170.33\,\mathrm{KeV}$, and $\eta(z) \equiv 1$. It is also assumed that the angular divergence of the incident photon beam is $1°$. Then, if the positron-emission activity of the radionuclide employed is 300 mCi, the mean sensing photon flux will be $q_0 \cong 1.68 \times 10^6$ s^{-1}. Also, the radius of the sensing beam in the soil will be about $3 - 5$ mm. Correspondingly, the
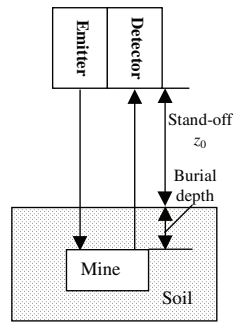

Figure 4. Illustration of landmine detection.

sampling step of the lateral scan employed to obtain 2D images of the probed medium is chosen to be 8 mm. The soil density is considered as varying along the LOS according the law

$$\rho(z) = \rho_n f(z - z_0), \tag{7}$$

where $\rho_n = 1.3 \, \text{g/cm}^3$, and function $f(z) = 1 + (z/z_\text{p}) \exp(-z/z_\text{p})$ describes the density variations along the LOS; $f(z) \equiv 0$ at $z < 0$. Assume also that $z_\text{p} = 1$ cm. The composition of the soil, and its basic density, extinction and backscattering coefficients are given in Table 1. The landmine is assumed to

Table 1. Characteristics of soil, TNT and Bakelite used in the simulations.

	Soil	**TNT**	**Bakelite**
Element	**Fraction by weight (%)**		
H	2.1	2.2	5.7
C	1.6	37.0	77.5
N		18.5	
O	57.7	42.3	16.8
Al	5		
Si	27.1		
K	1.3		
Ca	4.1		
Fe	1.1		
Density $[g/cm^3]$	1.3	1.6	1.25
$\alpha \, [m^{-1}]$	29.2	36.603	28.54
$\beta_\mathbf{c} \, [m^{-1}/sr]$	0.588	0.748	0.584

be a cylindrical, 8 mm thick plastic casing containing pure TNT as explosive with sizes approximating those as in real mines of Type 72: 6.4 cm in diameter and 3 cm in height. The characteristics of the plastic (bakelite) and TNT are also given in Table 1. The detection and recognition of such a type of mines is relatively most difficult because of their non-metallic casing and minimum sizes, and the lower density of TNT ($1.6 \, \text{g/cm}^3$) compared to that of RDX ($1.8 \, \text{g/cm}^3$). The mine sample is considered as buried (in the soil) in different depths $D = (z - z_0)$, gradually increasing from $D = 1$ cm to $D = 15$ cm, where the soil density has different values. Let us note here (see also Table 1) that the values of the extinction and backscattering coefficients, respectively, of soil, $\alpha(z)$ and $\beta(z)$, bakelite, α_b and β_b, and explosive (TNT), α_e and β_e, are determined mainly by the material density. Correspondingly, the contrast $\delta_\text{c}\alpha_{\text{b,e}}(z) = (\alpha_{\text{b,e}} - \alpha(z))/\alpha_{\text{b,e}}$ between α_b or α_e and $\alpha(z)$ will be mainly determined by (practically equal to) the contrast $\delta_\text{c}\rho_{\text{b,e}}(z) = (\rho_{\text{b,e}} - \rho(z))/\rho_{\text{b,e}}$ between the soil density $\rho(z)$ and the density ρ_b or ρ_e of bakelite or TNT. According to the model accepted of soil density [Eq.(7)] and the data given in Table 1, the values of $\delta_\text{c}\alpha_\text{b}$ and $\delta_\text{c}\alpha_\text{e}$ are obtained to be -0.175 and 0.083 at
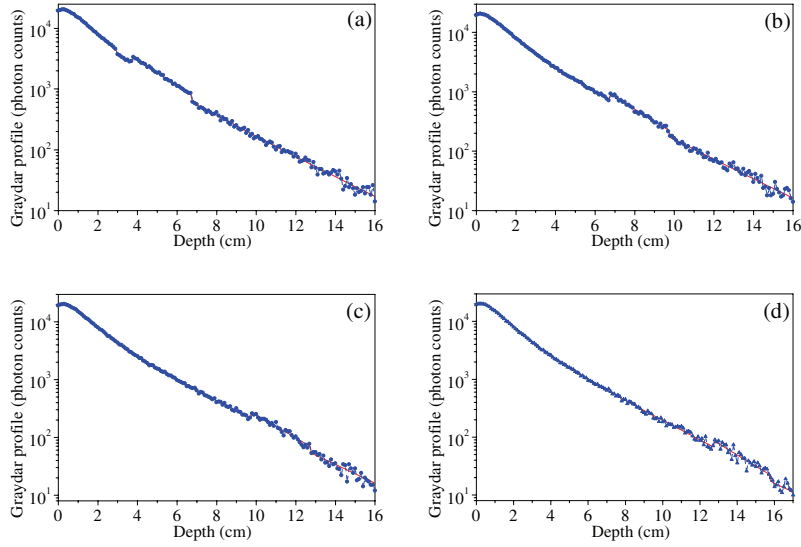
Figure 5. Realizations of the graydar profiles (compared with the expected ones given by solid curves) obtained at mine burial depths of 3 cm (a), 6 cm (b), 9 cm (c), and 12 cm (d).

$D = 3$ cm, -0.038 and 0.19 at $D = 6$ cm, and -0.024 and 0.20 at $D = 9$ cm and 12 cm. The corresponding values of $\delta_c\rho_b$ and $\delta_c\rho_e$ are -0.195 and 0.066 at $D = 3$ cm, -0.055 and 0.176 at $D = 6$ cm, -0.04 and 0.187 at $D = 9$ cm and 12 cm. Since the thickness of the plastic casing is relatively small, at large depths and low density contrast between bakelite and soil ($|\delta_c\rho_b| < 5\%$ at $D > 5$ cm) it might be impossible to distinguish the casing. Then the task to be solved would consist in the detection and recognition of the explosive TNT alone. The corresponding simulated logarithmic graydar profiles along the LOS, obtainable for $T = 100$ s are shown in Figure 5, where one can see the regions of linear decrease of $\ln S$ [$\ln N_T(E_{bc}, z, \Delta z)$] for bakelite (at $D = 3$ cm) and TNT. The recovered profiles of extinction are compared with the premised models in Figure 6. One may notice here that at a depths between 0.4 and 2 cm the soil density should exceed that of bakelite and TNT. The differences (deviations) obtained $\widehat{\delta\alpha_b} = \alpha_{br} - \alpha_b$ and $\widehat{\delta\alpha_e} = \alpha_{er} - \alpha_e$ between the recovered values, α_{br} and α_{er}, and the true (premised) ones, α_b and α_e, of bakelite and explosive (TNT), respectively, are $\widehat{\delta\alpha_b} = 2.83$ m^{-1} and $\widehat{\delta\alpha_e} = -0.95$ m^{-1} at $D = 3$ cm, $\widehat{\delta\alpha_e} = 0.37$ m^{-1} at $D = 6$ cm, $\widehat{\delta\alpha_e} = 0.76$ m^{-1} at $D = 9$ cm, and $\widehat{\delta\alpha_e} = -1.7$ m^{-1} at $D = 12$ cm. These values are lying within the interval $[-2\delta\alpha_{b,e}, 2\delta\alpha_{b,e}]$, where $\delta\alpha_{b,e}$ is the rms error [evaluated on the basis of Eq.(3)] in the determination of the extinction coefficient α_b or α_e. The corresponding relative errors $\widehat{\delta_r\alpha_b} = \widehat{\delta\alpha_b}/\alpha_b$ and $\widehat{\delta_r\alpha_e} = \widehat{\delta\alpha_e}/\alpha_e$ are $\widehat{\delta_r\alpha_b} = 10\%$
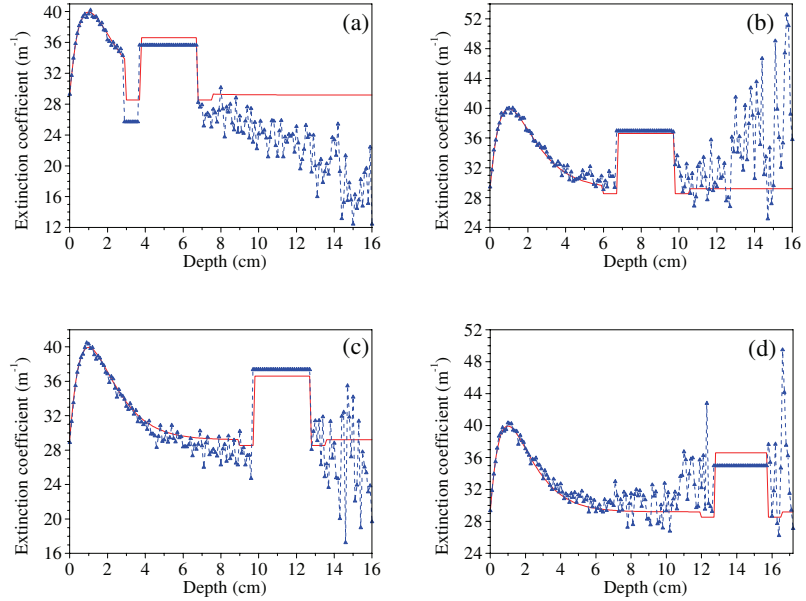
Figure 6. Recovered profiles of the extinction coefficient (triangles) compared with the models corresponding to the graydar profiles given in Figure 5.

(at $D = 3$ cm) and $\widehat{\delta_r \alpha_e} = 2.5\%$ (at $D = 3$ cm), 1% (at $D = 6$ cm), 2% (at $D = 9$ cm), and 5% (at $D = 12$ cm). Thus, it turns out that α_b and α_e may be determined with a relatively high accuracy allowing one to detect, locate, and recognize a mine at relatively low values of the contrast $\delta_c \alpha_{b,e}$ or $\delta_c \rho_{b,e}$ (see above). One should note as well that the mine is detectable and clearly discernible even at depths of 15 cm, without any noticeable shadowing effect of the preceding (along the LOS) soil layers with higher density.

An interesting result from the simulations performed is revealing the behaviour of the error in the determination of the extinction (density) distribution of soil (or other surrounding substance) along a LOS intersecting homogeneous one-material ingredients. Like in the absence of ingredients [16], the statistical rms error $\delta_s \alpha(z) = \langle [\alpha_r(z) - \langle \alpha_r(z) \rangle]^2 \rangle^{1/2}$ is accumulated and increases with increasing z, due to the recurrent character of algorithm (4). At the same time, depending on the concrete realization of the graydar profile, a positive or negative bias $\delta_b \alpha(z) = \langle \alpha_r(z) \rangle - \alpha(z)$ may arise with more or less sharply increasing (with z) module $|\delta_b \alpha(z)|$ (see Figures 6 and 7). It is seen in the Figures that the bias module is of the order of the range of the fluctuations of $\alpha_r(z)$ (see also [16]). Therefore, the bias visibly arises at some depth where the fluctuations of $\alpha_r(z)$ become noticeable. For some realizations of the graydar profile there is no bias (Figure 7, asterisks). In such cases the natural bias, that is intrinsic to
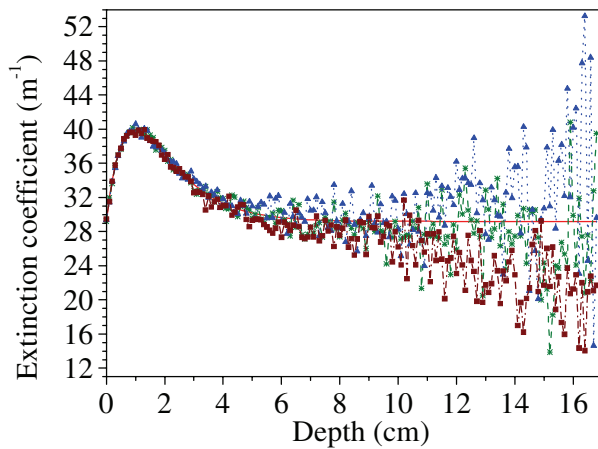
Figure 7. Recovered profiles of the extinction coefficient (compared with the expected one) for three realizations of the graydar profile for soil without mine.

non-linear inverse algorithms like Eq.(4), is as if compensated for in any way. In any case, the above-described chaotic behaviour of the recovered profile $\alpha_r(z)$ would be of interest as an independent mathematical problem.

The results from simulating the procedure of obtaining a 2D (tomographic) image (vertical diametrical section) of a mine buried in depth of $D = 6$ cm in soil are illustrated in Figure 8. The simulation consists in reproducing a lateral scan with $T = 100$ s per one position of the LOS and scanning step of 8 mm. To avoid considering the inessential by now boundary effect, we suppose that the diameter of the sensing gamma-ray beam is exactly integer times involved by both the radial thickness of the mine casing and the radius of the TNT bar. It is seen in Figure 8 that the mine shape and material contents are well discernible.

The simulations performed for the case of a longer measurement time T and/or a higher incident photon rate q_0 (a greater statistical volume $q_0 T$) demonstrated the expected higher efficiency of the graydar sensing. So, at $T = 200$ s or 1000 s a mine is detectable and discernible (with accuracy and contrast near those at $T = 100$ s) to greater depths. The corresponding depths of arising a bias in the determination of $\alpha(z)$ [$\rho(z)$] are also greater compared to the case when $T = 100$ s. At fixed depths the sensing accuracy is perceptibly increased with increasing T. As a result, a better quality is achieved of the recovered 2D images of the mine explosive.
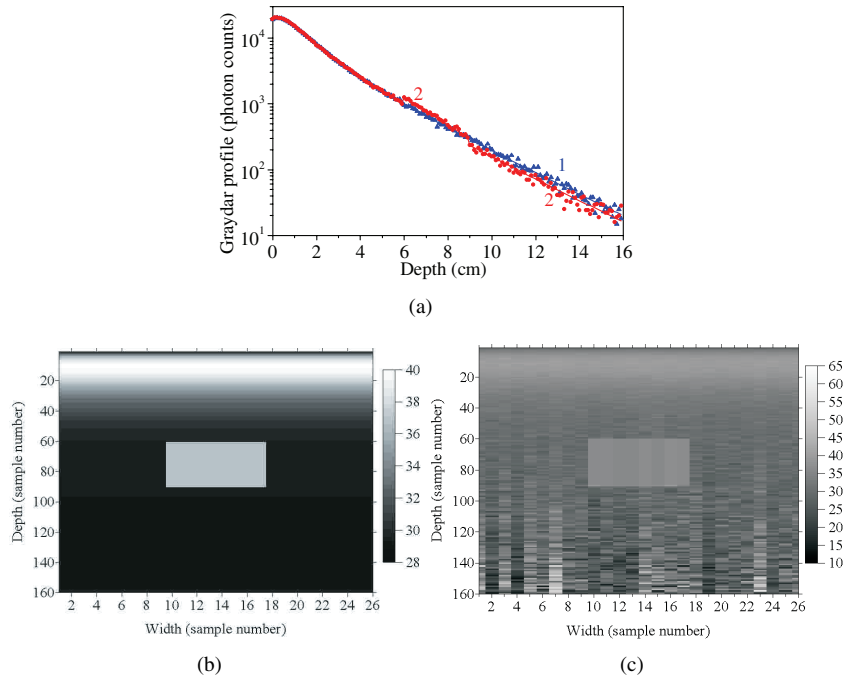
(a)

(b)

(c)

Figure 8. (a) LOS graydar profiles obtained without (1) and with (2) a mine. Model (b) and recovered (c) 2D extinction image (vertical diametrical section) of a mine buried in soil. The grey level bar is in units of m^{-1}.

5   Conclusion

In this work, after a brief review on the leading ideas and some recent results concerning the graydar approach to sensing dense, optically opaque media, we investigated analytically and by simulations a new case of probed medium compared to those considered formerly. In this case the medium to be evaluated consists of one-material surroundings with non-uniform density distribution containing homogeneous one-material ingredients. A working formula [Eq.(4)] was derived for recovering the profiles of the extinction and backscattering coefficients of the surrounding medium when the LOS penetrates different homogeneous ingredients. The simulations conducted confirmed the validity of Eq.(4) and showed that under Poisson noise conditions one could detect, locate, and accurately distinguish and recognize the explosive of a plastic TNT landmine buried in soil with non-uniform density distribution. The duration of the measurement procedure per one LOS was supposed to be 100 s at 1.68×10^6 photons/s incident photon flux (300 mCi positron emission activity of the radionuclide employed at 1° angular divergence of the sensing pho-

ton beam). The simulated longitudinal (along the LOS) and transversal sensing resolution was, respectively, 1 mm and 8 mm. A relatively high recognition accuracy has been achieved ($< 5\%$) at burial depths of 3 cm to 15 cm and a relatively low extinction or density contrast ($8 - 20\%$). Thus, even at a relatively large depth of 15 cm (weak return signal) a mine is detectable and clearly discernible without noticeable shadowing effect of the upper soil layers having a higher peaky-shaped density.

Also, the results from simulations revealed an interesting effect observed formerly [16] and following from the non-linear recurrent character of the algorithm [Eq.(4)] for retrieving the profile $\alpha(z)$ of the extinction coefficient of the surrounding medium. The effect consists in that, except the expected accumulation of the statistical error with increasing z, a chaotic bias in the determination of $\alpha(z)$ may arise and become visible at some depth of sensing. Depending on the concrete realization of the graydar profile, the bias may be positive or negative and more or less sharply increasing with increasing z. In some cases the bias is absent. Such a chaotic instability in the behaviour of the recovered profiles $\alpha_{\mathrm{r}}(z)$ could be of an independent mathematical interest.

As a whole, from a somewhat idealized point of view based on considering the Poisson noise alone, one may conclude that it is possible to realize single-sided gamma-ray in-depth sensing and tomography of dense one-material optically-opaque media with non-uniform density distribution and homogeneous one-material ingredients inside. In light materials like soil (with density of 0.9 to $1.9\,\mathrm{g/cm^3}$) one may find and identify low-contrast ingredients, such as explosive TNT having a density of $1.6\,\mathrm{g/cm^3}$, to depths of about 15 cm. In this case the measurement time per one LOS may be of the order of 100 s at $10^6 - 10^7$ photons/s intensive beams of sensing gamma photons (of energy $511\,\mathrm{KeV}$). Since the light materials contain mainly light elements (Table 1), the Doppler broadening of the Compton energy would be negligibly small and would not affect essentially the energy selection of the signal photons and thus the rejection of the parasitic photons due to background and multiple lateral scattering. The problem about the timing uncertainty when measuring the arrival time of the signal photons is technological and is connected with the development of fast data acquisition and processing techniques.

A common natural result following from the simulations performed is that increasing the measurement time T and/or the sensing photon flux q_0 (*i.e.*, increasing the statistical volume $q_0 T$) leads to enlargement of both the depths of accurate detection and evaluation of ingredients and the depth of arising a bias of the recovered LOS density distribution of the surrounding medium. At a fixed depth the sensing accuracy increases, which leads to a better quality of the obtained images of the probed medium and a better discernability of different ingredients of interest.

*L.L. Gurdev, T.N. Dreischuh, D.V. Stoyanov, Ch.N. Protochristov*

Acknowledgments

References

[1] G. Hertz (1966) *Lehrbuch der Kernphysik I (Experimentalle Verfahren)*, B.G.Teubner Verlagsgesellshaft, Leipzig.

[2] J. M. Jauch and F. Rohrlich (1976) *The Theory of Photons and Electrons*, Springer, New York.

[3] J. H. Hubbell, and S. M. Seltzer (2004) *Tables of X-Ray Mass Attenuation Coefficients and Mass Energy-Absorption Coefficients* (version 1.4). [Online] Available: http://physics.nist.gov/xaamdi, MD: National Institute of Standards and Technology, Gaithersburg.

[4] J. A. Stokes et al. (1982) *Nucl. Instr. and Meth.* **193** 261.

[5] G. Harding and J. Kosanetzky (1989) *Nucl. Instr. and Meth. A* **280** 517.

[6] P. Zhu, P. Duvauchelle, G. Peix, and D. Babot (1996) *Meas. Sci. Technol.* **7** 281.

[7] S. J. Norton (1994) *J. Appl. Phys.* **76** 2007.

[8] N. V. Arendtsz and E. M. A. Hussein (1995) *IEEE Trans. Nucl. Sci.* **42** 2155.

[9] N. V. Arendtsz and E. M. A. Hussein (1995) *IEEE Trans. Nucl. Sci.* **42** 2166.

[10] B. L. Evans et al., (1998) *IEEE Trans. Nucl. Sci.* **45** 950.

[11] B. L. Evans, J. B. Martin et al. (2002) *Nucl. Instr. and Meth. A* **480** 797.

[12] R. S. Thoe (1996) *Rev. Sci. Instrum.* **67** 89.

[13] G. Herman (1980) *Image Reconstruction from Projections. The Fundamentals of Computerized Tomography*, Academic Press, New York.

[14] F. Natterer (1986) *The Matematics of Computerized Tomography*, Wiley, Chichester.

[15] B. Gustafsson (1996) *Physica Scripta* **T61** 38.

[16] L. L. Gurdev, D. V. Stoyanov, T. N. Dreischuh, Ch. N. Protochristov, O. I. Vankov (2007) *IEEE Trans. Nucl. Sci.* **54** 262.

[17] T. N. Dreischuh, L. L. Gurdev, D.V. Stoyanov, Ch. N. Protochristov, O. I. Vankov (2007) *AIP Conference Proceedings - BPU6*, in print.

[18] T. N. Dreischuh, L. L. Gurdev, D.V. Stoyanov, Ch. N. Protochristov (2007) *Proc. SPIE* **6604**, in print.

[19] V. E. Radko (1991) *Instr. and Exper. Techn.* **34** 929.

[20] J. Gerl, F. Ameil, I. Kojouharov, and A. Surowiec (2004) *Nucl. Instr. and Meth. A* **525** 328.

[21] P. P. Kane (1997) *Radiat. Phys. Chem.* **50** 31.

[22] M. Schumacher (1969) *Phys. Rev.* **182** 7.

[23] W. Galbraith and W. S. C. Williams (Eds.) (1964) *High Energy and Nuclear Physics Data Handbook*, National Institute for Research in Nuclear Science and Rutherford High Energy Laboratory, Chilton.

[24] K.F. Eckerman and J.C. Ryman (1993) *External Exposure to Radionuclides in Air, Water, and Soil, Federal Guidance Report No. 12*, U.S. Environmental Protection Agency, Washington, D.C.
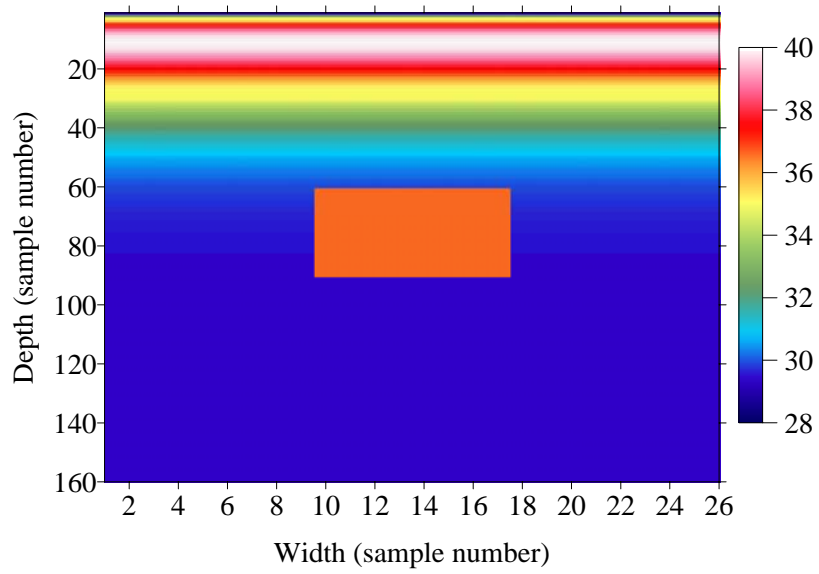
(b)
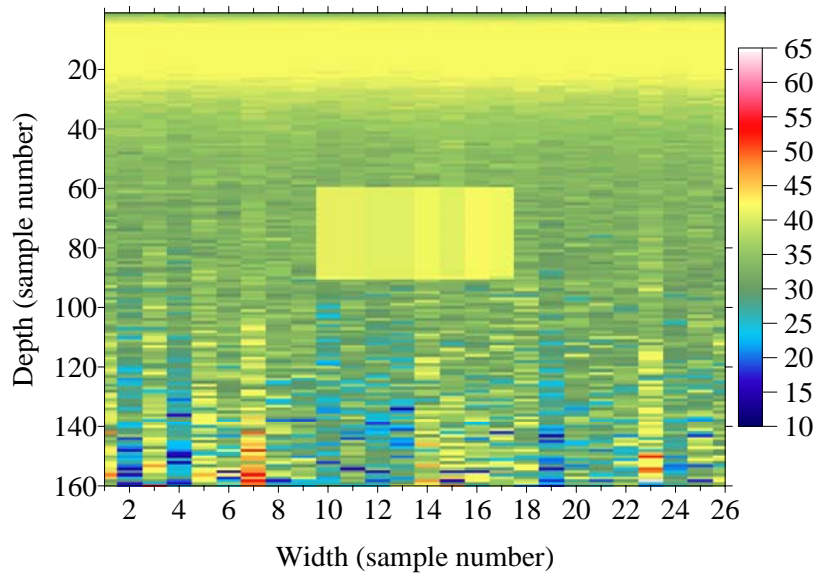
(c)

Figure 8. Model (b) and recovered (c) 2D extinction image (vertical diametrical section) of a mine buried in soil. The level bar is in units of m^{-1}.